Hydrol. Earth Syst. Sci. Discuss., 12, 5749–5787, 2015
www.hydrol-earth-syst-sci-discuss.net/12/5749/2015/
doi:10.5194/hessd-12-5749-2015

Hydrology and Earth System Sciences
Open Access
Discussions

Correction of real-time satellite precipitation with satellite soil moisture observations

W. Zhan[1], M. Pan[1], N. Wanders[2], and E. F. Wood[1]

[1]Department of Civil and Environmental Engineering, Princeton University, Princeton, NJ, USA
[2]Department of Physical Geography, Utrecht University, Utrecht, the Netherlands

Received: 28 April 2015 – Accepted: 19 May 2015 – Published: 16 June 2015

Correspondence to: W. Zhan (wzhan@princeton.edu)

Published by Copernicus Publications on behalf of the European Geosciences Union.

Abstract

Rainfall and soil moisture are two key elements in modeling the interactions between the land surface and the atmosphere. Accurate and high-resolution real-time precipitation is crucial for monitoring and predicting the on-set of floods, and allows for alert and warning before the impact becomes a disaster. Assimilation of remote sensing data into a flood-forecasting model has the potential to improve monitoring accuracy. Space-borne microwave observations are especially interesting because of their sensitivity to surface soil moisture and its change. In this study, we assimilate satellite soil moisture retrievals using the Variable Infiltration Capacity (VIC) land surface model, and a dynamic assimilation technique, a particle filter, to adjust the Tropical Rainfall Measuring Mission Multi-satellite Precipitation Analysis (TMPA) real-time precipitation estimates. We compare updated precipitation with real-time precipitation before and after adjustment and with NLDAS gauge-radar observations. Results show that satellite soil moisture retrievals provide additional information by correcting errors in rainfall bias. High accuracy soil moisture retrievals, when merged with precipitation, generally increase both rainfall frequency and intensity, and are most effective in the correction of rainfall under dry to normal surface condition while limited/negative improvement is seen over wet/saturated surfaces. Errors from soil moisture, mixed among the real signal, may generate a false rainfall signal approximately 2 mm day^{-1} and thus lower the precipitation accuracy after adjustment.

1 Introduction

Precipitation is perhaps the most important variable in controlling energy and mass fluxes that dominate climate and particularly the terrestrial hydrological and ecological systems. Precipitation estimates, together with hydrologic models, provide the foundation for understanding the global energy and water cycles (Sorooshian, 2004; Ebert et al., 2007). However, obtaining accurate measurements of precipitation at regional to

HESSD
12, 5749–5787, 2015

global scales has always been challenging due to its small-scale, space–time variability, and the sparse networks in many regions. Such limitations impede precise modeling of the hydrologic responses to precipitation. There is a clear need for improved, spatially distributed precipitation estimates to support hydrological modeling applications.

In recent years, remotely sensed satellite precipitation has become a critical data source for a variety of hydrological applications, especially in poorly monitored regions such as sub-Saharan Africa due to its large spatial coverage. To date, a number of fine-scale, satellite-based precipitation estimates are now in operational production. One of the most frequently used is the Tropical Rainfall Measuring Mission Multi-satellite Precipitation Analysis (TMPA) product (Huffman et al., 2007). Over the 17 years lifetime since the launch of the Tropical Rainfall Measuring Mission (TRMM) in 1997, a series of high resolution (0.25° and 3 hourly), quasi-global (50° S–50° N), near-realtime, TRMM-based precipitation estimates have been developed and made available to the research and applications communities (Huffman et al., 2007, 2010). Flood forecasting and monitoring is one major application for real time satellite rainfall products (Wu et al., 2014). However, the applicability of satellite precipitation products for near real-time hydrological applications that include drought and flood monitoring has been hampered by their need for gauge-based adjustment.

While it is possible to create such estimates solely from one type of sensor, researchers have increasingly moved to using combinations of sensors in an attempt to improve accuracy, coverage and resolution. A promising avenue for rainfall correction is through the assimilation of satellite-based surface soil moisture into a water balance model (Pan and Wood, 2006). Over land, the physical relationship between variations in soil water storage and rainfall accumulation contain complementary information that can be exploited for the mutual benefit of both types of products (Massari et al., 2014; Crow et al., 2009). Unlike instantaneous rain rate, satellite surface soil moisture retrievals utilize low frequency microwave signals and possess some memory reflecting antecedent rainfall amounts.

HESSD
12, 5749–5787, 2015

Studies have demonstrated that in situ (Brocca et al., 2009, 2013; Matgen et al., 2012) and satellite (Francois et al., 2003; Pellarin et al., 2008, 2013; Brocca et al., 2014) estimates of surface soil moisture could contribute to precipitation estimates by providing useful information concerning the sign and magnitude of antecedent rainfall accumulation errors. In particular, Brocca et al. (2014) estimated daily rainfall on a global scale based on satellite SM products by inverting the soil water balance equation. Crow et al. (2003, 2009, 2011) corrected spaceborne rainfall retrievals by assimilating remotely sensed surface soil moisture retrievals into a simple soil water balance model using a Kalman filter (Kalman, 1960). The hydrologic response of soil moisture to precipitation is especially important in that an explicit and sophisticated physical model is needed to accurately recover spatial information about the rainfall more precisely, e.g. wetted area. This is because most storm systems have a very strong and complicated spatial structure that is non-Gaussian and non-stationary in both time and space (Wanders et al., 2015).

In this paper we present a method to improve real-time remote sensing precipitation products by merging retrievals with soil moisture remote sensing products through a Particle Filter (PF), and therefore offer an improved basis for quantitatively monitoring and predicting flood events, especially in those parts of the world where in-situ networks are too sparse to support more traditional methods of hydrologic monitoring and prediction. The precipitation enhancement experiments are carried out over the continental US (CONUS) and the precipitation skill is validated against the NLDAS gauge-radar precipitation product.

2 Methods

2.1 Overview

Random replicates of satellite precipitation are generated based on real-time TMPA (3B42RT) retrievals and its uncertainty (Pan et al., 2010), which are then used to

HESSD
12, 5749–5787, 2015

force the VIC land surface model (LSM) where one output of interest is surface soil moisture. Satellite soil moisture data products are compared and merged with the TMPA (3B42RT) product to improve the accuracy of the satellite precipitation estimates. A schematic for the study approach is provided in Fig. 1. Based on real-time TMPA (3B42RT) retrievals, a set of possible precipitation estimates (a.k.a. replicates or particles) $\{p^i\}_{i=1,2,\ldots,N}$ is generated with assigned initial prior probability weights $\{w^i\}_{i=1,2,\ldots,N}$. These rainfall rates are then used to force the VIC land surface model to produce soil moisture predictions $\{\theta^i\}_{i=1,2,\ldots,N}$. Retrievals of AMSR-E satellite surface soil moisture using the Land Surface Microwave Model (LSMEM) (Pan et al., 2014) are then merged with the LSM-based soil moisture within the Particle Filter (PF) that compares AMSR-E/LSMEM changes in soil moisture, ΔSM, to the LSM predicted soil moisture changes. From these, posterior weights $\{w^{i+}\}_{i=1,2,\ldots,N}$ are calculated for each precipitation member (particle) that takes into account the uncertainties of AMSR-E/LSMEM ΔSM retrievals. From these updated weights, an updated precipitation probability distribution is constructed, where the precipitation particle with highest probability is taken as the "best" adjusted precipitation estimate ($3B42RT_{ADJ}$). The procedure is carried out over the continental US (CONUS) region on a grid-by-grid basis (0.25°) and a daily time step. Allowing for 6 months model spin-up period, the adjustment is done from January 2003 to July 2007.

2.2 Modeling, statistical tools and data sources

2.2.1 The particle filter

Data assimilation methods are capable of dynamically merging predictions from a state equation (i.e. the land surface model) with measurements (i.e. AMSR-E retrievals) to minimize uncertainties from both the predictions and measurements. It is assumed that the source of uncertainty in the land surface model predictions come solely from the real-time satellite precipitation, so that the particle filter (PF) provides an algorithm

HESSD
12, 5749–5787, 2015

to update the precipitation based on the AMSR-E retrievals. The state evolution of a particle filter from discrete time $t-1$ to t can be represented as:

$$\theta_t = f_t\left(\theta_{t-1}, p_t, \kappa_t, \alpha_t\right) \tag{1}$$

where θ_t is the 1st layer soil moisture at time t, whose value is predicted by the state equation Eq. (1) as $f_t(\bullet)$, and in the study is the hydrological model VIC, which takes in forcing data, including precipitation (p_t) and other forcings (κ_t); and simulates land surface states (soil moisture and soil temperatures at various levels, snow, etc.) and fluxes (evapotranspiration, runoff) at time t. Herein we are basically interested only in the 1st layer (top 10 cm) soil moisture state and precipitation forcing, so other states and fluxes are not explicitly shown. α_t is the random error in the prediction of θ_t, whose statistics are known but not its value at any specific time.

At time t, the satellite surface soil moisture retrieval, θ_t^*, can be related to the VIC modeled 1st layer soil moisture θ_t as:

$$\theta_t^* = h_t\left(\theta_t, \beta_t\right) \tag{2}$$

where h_t is taken as a regression that transforms the VIC simulated 1st layer soil moisture to satellite surface soil moisture. β_t is the noise in this regression relationship. The two noises α_t and β_t are assumed to be independent of each other at all times t.

At time t, given a TMPA (3B42RT) precipitation estimate, p_t^{sat}, a set of N precipitation replicates $\{p_t^i\}_{i=1,2,\ldots,N}$ and their associated initial prior probability weight $\{w_t^i\}_{i=1,2,\ldots,N}$ are generated.

$$g\left(p_t^{\text{sat}}\right) \sim \left\{p_t^i, w_t^i\right\}_{i=1,2,\ldots,N} \tag{3}$$

$$\sum_{i=1}^{N} w_t^i = 1 \tag{4}$$

HESSD
12, 5749–5787, 2015

$g(\,)$ is a probability density function. For N precipitation replicates, $\{p_t^i\}_{i=1,2,\ldots,N}$, the propagation of the states from time step $(t-1)$ to t is by the VIC land surface model represented in Eq. (1). The VIC land surface model simulates the 10 cm 1st layer soil moisture, $\{\theta_t^i\}_{i=1,2,\ldots,N}$ for each precipitation replicate.

$$\left\{\theta_t^i = f_t\left(\theta_{t-1}, p_t^i, \kappa_t, \alpha_t\right)\right\}_{i=1,2,\ldots,N} \tag{5}$$

with the associated weights assigned to the precipitation member:

$$\left\{\theta_t^i, w_t^i\right\}_{i=1,2,\ldots,N} = \left\{f_t\left(\theta_{t-1}, p_t^i, \kappa_t, \alpha_t\right), w_t^i\right\}_{i=1,2,\ldots,N} \tag{6}$$

If the satellite soil moisture retrieval at time t is θ_t^*, the update of precipitation forcing is accomplished by updating the importance weight of each replicate given the "measurement" θ_t^*:

$$w_t^{i+} \sim \left\{g\left(\theta_t^i|\theta_t^*\right)\right\}_{i=1,2,\ldots,N} \tag{7}$$

$$\sum_{i=1}^{N} w_t^{i+} = 1 \tag{8}$$

The likelihood function $g\left(\theta_t^i|\theta_t^*\right)$ can be derived from h_t and $g(\beta_t)$. The schematic of the utilized strategy is shown in Fig. 2. The primary disadvantage of the particle filter is the large number of replicates required to accurately represent the conditional probability densities of p_t and θ_t. When the measurements exceed a few hundred, the particle filter is not computationally practical for land surface problems. Considering computation efficiency, we set the number of independent particles, N, from the prior distribution to be 200.

HESSD
12, 5749–5787, 2015

2.2.2 Precipitation replicates generation

We generate precipitation replicates, $\{p_t^i\}_{i=1,2,\ldots,N}$, based on statistics comparing NLDAS and TMPA (3B42RT) precipitation, as shown in Fig. 3. Given a TMPA (3B42RT) precipitation measurement (binned by magnitude), with bin minimum and maximum indicated in Fig. 3, precipitation replicates are generated based on the corresponding 15th, 30th, 70th, 85th percentiles and the maximum NLDAS precipitation of the particular quantile bin as follows: 15 % of the replicates are generated with values uniformly distributed from 0 and 15th percentile; 15 % of replicates with values from 15th to 30th percentile; 20 % of replicates with values from 30th percentile to the median; 20 % of the replicates generated from the median to 70th; 15 % with values from 70th to 85th percentile; and 15 % from the 85th percentile to the maximum precipitation value.

2.2.3 AMSR-E/LSMEM soil moisture retrievals

The soil moisture product is derived from multiple microwave channels of the Advanced Microwave Scanning Radiometer for EOS (AMSR-E) instrument. The retrieval algorithm by Pan et al. (2014) is an enhanced version of the Land Surface Microwave Emission Model (LSMEM). The near surface soil moisture and vegetation optical depth (VOD) are estimated simultaneously from a dual polarization approach that utilizes both horizontal (H) and vertical (V) polarizations measurement by the space-borne sensor. The input AMSR-E brightness temperature comes from the NSIDC AMSR-E/Aqua Daily Global Quarter-Degree Gridded Brightness Temperatures product (overlapping swaths in the same day are truncated so that only the latest one is present). Consequently, the soil moisture retrievals are also gridded at 0.25° with one ascending map and one descending map at the daily time step. A maximum threshold value of $0.6\,m^3\,m^{-3}$ has been applied manually to reduce error from open water bodies. According to Pan et al. (2014), the soil moisture dataset based on observations from AMSR-E are shown to be consistent at large scales in terms of reproducing the spatial pattern of soil moisture from VIC land surface model simulation. Descending soil

HESSD
12, 5749–5787, 2015

moisture retrievals (equatorial crossing time 01:30 LT) have better accuracy than ascending map (equatorial crossing time 13:30 LT) since the atmospheric and surface temperature conditions are much more stable in the morning.

Similarly, while the spatial patterns of the basic statistics of AMSR-E/LSMEM SM retrievals compare well to VIC simulations (Pan et al., 2014), VIC has its top layer (10 cm), which is deeper than the detection depth of AMSR-E, so that the mean and temporal variability of the retrievals are higher than the VIC simulated soil moisture (Fig. 4 in Pan et al., 2014). Considering this difference between detection depths, we pre-process soil moisture retrievals as follows:

1. Rescale soil moisture retrievals (AMSR-E/LSMEM SM) to have the same minimum and maximum range as VIC simulated 1st layer soil moisture.

2. Calculate a daily soil moisture change. As satellite retrievals are manually truncated to be no more than 0.6 $m^3 m^{-3}$ (equivalent to 60 mm of water in the top soil layer in VIC), retrievals larger than 0.6 $m^3 m^{-3}$ are excluded.

3. Fit a 2nd order polynomial regression model with ΔSM (all units in mm of water in the top layer) from satellite and VIC simulation on a monthly basis and 3 × 3 grid scale (window).

After pre-processing, the distribution of soil moisture change matches fairly well with ΔSM_{VIC} (Fig. 4). The mean absolute difference of soil moisture change before and after pre-processing, compared to ΔSM_{VIC}, is shown in Fig. 5. The mean absolute difference reduces from a spatial average of 5.25 mm day^{-1} (Fig. 5a) to 0.71 (Fig. 5b) mm day^{-1}, with relatively larger value over eastern CONUS. According to Pan et al. (2014), the no-skill or negative-skill areas occur mostly over eastern dense forests due to vegetation blockage of the soil moisture signal (Pan et al., 2014). The accuracy of soil moisture retrievals is also limited by mountainous topography and the occurrence of snow and frozen ground during winter whose identification from satellite observations is often difficult. For the purpose of this study, we assign zero weight to the TMPA ($3B42RT_{ADJ}$)

HESSD
12, 5749–5787, 2015

and rely exclusively on the initial TMPA (3B42RT) precipitation for time steps when the VIC model predicts snow cover or frozen surfaces.

2.2.4 VIC land surface model

The Variable Infiltration Capacity (VIC) model (Liang et al., 1994; Gao et al., 2010) is used to dynamically simulate the hydrological responses of soil moisture to precipitation, surface radiation and surface meteorology. The VIC model solves the full energy and water balance over each 0.25°-grid-cell independently, thus ensuring its computational efficiency. Three-layer-soil-moisture is simulated through a soil–vegetation–atmosphere transfer (SVAT) scheme, which also accounts for sub-grid scale heterogeneity of vegetation, soil and topography. A detailed soil moisture algorithm description can be found in Liang et al. (1996). The VIC model has been validated extensively over CONUS by evaluating soil moisture and simulations to observations (Robock et al., 2003; Schaake et al., 2004).

3 Idealized experiment

Before applying the Particle Filter assimilation algorithm on TMPA (3B42RT) precipitation estimates, we conducted an idealized experiment where we treat the NLDAS precipitation as the "truth" and the NLDAS precipitation forced VIC simulations as "satellite observed" soil moisture. As an idealized experiment, we adjust TMPA real-time precipitation estimates based on these "satellite observations". Phase 2 of the North American Land Data Assimilation System (NLDAS-2) rainfall forcing combines hourly WSR-88D radar analyses from the National Weather Service (NWS) and daily gauge reports ($\sim 13\,000\,\mathrm{day}^{-1}$) from the Climate Prediction Center (CPC) (Ek et al., 2011). The dataset, with a spatial resolution of 0.125° and hourly observations, was pre-processed into 0.25° daily precipitation to be consistent with that of TMPA (3B42RT) and AMSR-E/LSMEM SM datasets. The idealized experiment is designed to test whether the al-

HESSD
12, 5749–5787, 2015

gorithm is able to retrieve rainfall forcing with soil moisture change, assuming that the soil moisture observations are 100 % accurate.

Results show that, with the knowledge of 1st layer soil moisture change (via the "satellite observations"), the adjustment is able to recover intensity and spatial pattern of forcing precipitation (Fig. 7). Average mean absolute error (MAE) of daily rainfall amount is reduced by 52.9 % (2.91 to 1.37 mm day^{-1}) over the region. Figure 6a to e shows an example of the recovered rainfall field from the idealized experiment for 27 October 2003. The spatial pattern matches the original NLDAS precipitation well.

3.1 Effect of surface soil saturation

While successfully recovering the general pattern of NLDAS precipitation based on first layer soil moisture, the idealize experiment is not always able to recover the precipitation volume due to the fact that the top layer soil moisture alone does not contain the complete memory of the previous day's rainfall. Deeper soil moisture, evapotranspiration and runoff also carry part of this information. As the surface gets wetter, the VIC 1st layer soil moisture has smaller variation. If the incoming precipitation brings the surface to saturation, the VIC model redistributes the soil moisture vertically though vertical moisture flow and generates runoff. Hence soil moisture increments, ΔSM, near saturation are less correlated with incoming precipitation as they change minimally to additional incoming rainfall. An example demonstrating this saturation effect is shown in Fig. 6f to j. When incoming precipitation brings the surface SM to (near) saturation, there is very limited improvement after the adjustment. Because of the low sensitivity of the soil surface to precipitation, there is little change in ΔSM in response to precipitation variations among the replicates. It is almost always the case that the algorithm is not able to find a "matching" ΔSM.

We separately evaluate the skill improvement in the recovered NLDAS precipitation with and without surface saturation (Fig. 8). The recovered precipitation, when the surface soil is saturated, only contributes more noise rather than an improvement to the rainfall estimates. The VIC model computes the moisture flow between soil layers using

HESSD
12, 5749–5787, 2015

an hourly time step. If the 1st layer soil moisture exceeds its maximum capacity, it is considered to be a surface saturation case. As seen in Fig. 6, there is very limited or negative skill in the recovered precipitation under saturated surface soil moisture conditions. Such circumstances are identified and the AMSR-E/LSMEM ΔSM observation disregarded by assigning zero weight to the TMPA ($3B42RT_{ADJ}$) values. Thus for wetter areas with heavy precipitation that potentially would bring the surface soil moisture to saturation, the TMPA (3B42RT) product is less likely to be adjusted according to satellite ΔSM and the best precipitation estimate is TMPA (3B42RT).

3.2 Effect of SM uncertainty

In the idealized experiment, NLDAS-VIC soil moisture is taken as truth with zero uncertainty associated with (θ_t^*). However, this assumption is not valid for real satellite SM retrievals, mean absolute error of which is approximately 3 % vol./vol. (McCabe et al., 2005). To consider this, we added error to the "truth" SM (normally distributed with standard deviations of 0.5, 1.0, 1.5, 2.0, 2.5, 3.0, 3.5, 4.0, 4.5 and 5.0 mm), and simulated the effect of SM uncertainty to evaluate the associated adjustment errors.

Figure 8 shows that larger soil moisture observation errors lead to larger error variation after adjustment. This also suggests that soil moisture responds to precipitation non-linearly based on different initial conditions. An estimated wetter surface has lower sensitivity to an incoming rainfall amount, resulting in larger error in the recovered NLDAS precipitation. As shown in Fig. 9, the error standard deviation of the recovered NLDAS precipitation increases with surface water content (statistics shown in Table 2). As we add noise larger than $N(0,0.5\,\text{mm})$ into "true" SM observation, there is a wet bias of approximately 1 mm day^{-1} regardless of 1st layer soil moisture level. This suggests that when the difference between 1st layer SM and saturation is less than 8 mm, the median of the errors in the recovered NLDAS precipitation grows from 0.16 to 1.89 mm day^{-1} when we add $N(0,5.0\,\text{mm})$ noise, while inter-quantile range (IQR) increases from 1.71 to 7.04 mm day^{-1}. Acknowledging such a wet bias, to avoid introducing any more unintentional bias in the TMPA ($3B42RT_{ADJ}$) estimates, we take as zero the uncertainty of

HESSD
12, 5749–5787, 2015

AMSR-E/LSMEM SM retrievals, i.e. we take $h_t(\theta_t,)$ as our single observation θ_t^* and adjust the TMPA (3B42RT) estimates accordingly.

It is noteworthy that the soil moisture change is calculated based on previous days' soil water contents. Therefore errors tend to accumulate over time until they are "re-set" when a significant precipitation event takes place. This type of uncertainty accounts for a small portion of the total error in the adjusted precipitation (black being the no error case in Fig. 9 with the "true" change in soil moisture from every time step). As complete global coverage is not provided with each orbit of the AMSR-E sensor, on average 44.01 % of the time steps during the study period have observations, with more frequent overpasses at higher latitudes (Fig. 10). This observation gap unavoidably introduces extra uncertainty in the retrieval of the precipitation signal. To further avoid possible additional errors, we update the forcing rainfall when a ΔSM temporal match (±0.4 mm) is available, and keep the original precipitation if a match isn't available.

4 Improvement on real-time precipitation estimates and their validation

Actual adjustment of the TMPA (3B42RT) retrievals based on AMSR-E/LSMEM ΔSM is carried out using the methods described in Sect. 2.2.3, and results from the idealized experiment (Sect. 3.3) with regard to the circumstances where an adjustment is applied. Figure 12 shows a snapshot of the rainfall field from the TMPA (3B42RT) product compared with NLDAS on 26 May 2006 and the adjusted rainfall pattern based on AMSR-E/LSMEM ΔSM. The TMPA ($3B42RT_{ADJ}$) rainfall field (Fig. 12b) is similar in terms of its spatial distribution compared to NLDAS precipitation estimates (Fig. 12d).

As shown in Fig. 11, TMPA (3B42RT) and AMSR-E/LSMEM ΔSM has a spatial average Pearson Correlation Coefficient of 0.37, compared to 0.52 for NLDAS. After the adjustment procedure, the Pearson correlation coefficient between the adjusted TMPA (3B42RT) and AMSR-E/LSMEM ΔSM increases to 0.53. There is a smaller increase in correlation over the western mountainous region, the Great Lakes region and east-

HESSD
12, 5749–5787, 2015

ern high vegetated and populated region. Additionally, the satellite soil moisture suffers from snow/ice/standing water contamination, which affects the potential for adjustment.

Figure 13 presents the basic statistics for TMPA (3B42RT) and TMPA (3B42RT$_{ADJ}$) averaged over the study period with the same statistics from NLDAS as a reference. In general, adjustment increases both rainfall amount and rain days. The TMPA (3B42RT$_{ADJ}$) has significant improvement over TMAP (3B42RT) in terms of long-term precipitation bias. The bias in TMAP (3B42RT) underestimated annual mean precipitation, which is reduced by 20.6 % from $-9.32\,\mathrm{mm\,month^{-1}}$ spatial average in TMAP (3B42RT) to $-7.40\,\mathrm{mm\,month^{-1}}$ in TMPA (3B42RT$_{ADJ}$). Frequency of rain days generally increases significantly everywhere, especially over the northern and eastern CONUS regions. The NLDAS data suggests an almost constant drizzling rainfall over parts of the western mountainous area (Montana, Idaho, Wyoming and Colorado), while assimilating AMSR-E/LSMEM ΔSM datasets does not have a signal of higher rainfall frequency. This is possibly due to lower soil moisture variability in satellite retrievals over the dry, mountainous areas and frequent presence of snow and ice (TMAP (3B42RT is not updated under such circumstances). Notably, given the frequency of satellite ΔSM observation (Fig. 10), such dramatic increase in time steps with rain suggests that AMSR-E/LSMEM ΔSM brings a large number of false rainfall signals. Since TMPA (3B42RT$_{ADJ}$) effectively corrects the long-term mean precipitation amount, it is likely that the excessive TMPA 3B42RT$_{ADJ}$) rainfall events could be coming from the high-frequency noise in AMSR-E/LSMEM soil moisture retrievals identified by Pan et al. (2004). The high frequency noise, up to $\pm 2\,\mathrm{mm\,day^{-1}}$, results in a TMPA (3B42RT$_{ADJ}$) error ranges (approx. $\pm 2\,\mathrm{mm\,day^{-1}}$ over a dry surface, Table 1).

Although more ΔSM observations are available in northern CONUS, there are also more days with snow cover or frozen ground where the adjustment algorithm does not update TMAP (3B42RT). There are more frequent occurrences of surface saturation over the eastern US since the region is generally wetter than the west, and as well there often has heavy summertime convective precipitation.

HESSD
12, 5749–5787, 2015

Figure 14 shows the assimilation results for the grids and days with soil moisture observations, using the NLDAS precipitation as a reference. Statistics are calculated from 3B42RT/3B42RT$_{ADJ}$ during days with valid satellite observation inputs and without surface snow, ice or saturation. Overall, the method is successful in correcting daily rainfall amount for 3B42RT precipitation $\geq 2\,mm\,day^{-1}$, given prior knowledge of an overestimated precipitation. Mean standard deviation (STD) of 3B42RT$_{ADJ}$–NLDAS is between 1 and $3\,mm\,day^{-1}$.

Figure 14 also suggests that prior knowledge of an overestimated precipitation event, satellite soil moisture assimilation is very effective in correcting satellite precipitation. Meanwhile, we see a larger standard deviation in TMPA (3B42RT$_{ADJ}$) with greater underestimation in TMPA (3B42RT), which typically brings the surface closer to saturation. However soil moisture increments are less sensitive to incoming precipitation on wetter soil. Therefore a ΔSM error often translates into TMPA (3B42RT$_{ADJ}$) in a magnified manner.

Spatially, the area with higher AMSR-E/LSMEM ΔSM accuracy lies primarily in mid to western US (Fig. 15). This is consistent with prior knowledge of the error characteristics of the AMSR-E/LSMEM SM product. In comparison, regions with relatively high retrieval confidence are non-mountainous regions with little urbanization. Over the rest of CONUS, mainly the east coast of US, improvement is not significant. Expectedly, enhancement is more significant in the former areas where lower errors are seen in the adjusted estimates with TMPA (3B42RT) $> 2\,mm\,day^{-1}$ (Fig. 15). The applied method is ineffective for light rainfall < 2 mm, for which the precipitation error distribution is shown in Fig. 16. Given TMPA (3B42RT) $< 2\,mm\,day^{-1}$, the adjustment tends to over-correct precipitation by adding excessive rainfall – probably due to the high frequency AMSR-E noise that was discussed previously so that most of the overestimation comes from satellite SM error rather than a rainfall signal. Further work is needed to better characterize this observation uncertainty and reduce the SM retrieval error so as to improve the satellite SM observation accuracy.

HESSD
12, 5749–5787, 2015

5 Conclusion and discussion

Based on the retrieved soil moisture from AMSR-E using the LSMEM model, we propose an assimilation procedure to integrate soil moisture information into the VIC land surface model so as to improve real-time, satellite precipitation estimates. The ability to detect rainfall events based on the original real-time precipitation estimates is now enhanced with the above improvements. The improved precipitation estimates, referred to as TMPA ($3B42RT_{ADJ}$) estimates, are overall consistent in reproducing the spatial pattern and time series of daily rainfall from NLDAS precipitation. The results illustrate the potential benefits of using data assimilation to merge satellite retrievals of surface soil moisture into a land surface model forced with real-time precipitation. Potentially the method can be applied globally for areas meeting vegetation cover and surface condition constraints that allows for soil moisture retrievals. Under these conditions, the approach can provide a supplementary source of information for enhancing the quality of satellite rainfall estimation, especially over poorly gauged areas like Africa.

Nonetheless, some caution is required. The results of this study shows that the adjusted real-time precipitation tends to add additional rain (frequency and rates) resulting in more time steps with rain and resulting in a slightly higher regional average. It is also noticed that the precipitation adjustments are insensitive with saturated soil moisture conditions. A wetter surface is more sensitive to any error associated with satellite observation by incorrectly adjusting the precipitation. These errors, mixed with the "real" signal, generally add approximately 1–2 mm of precipitation (or higher) depending on the satellite observation accuracy. It is important to consider these circumstances when observations are used so as to avoid introducing additional error. With these identified limitations, continued research is needed to assess the biases in the real-time precipitation retrievals on a local to regional basis so the assimilation system can be modified accordingly.

The assimilation scheme used here assumed that the errors were attributed to the real-time precipitation retrievals, but the precipitation estimates after adjustment in-

HESSD
12, 5749–5787, 2015

cludes errors from additional sources. The two primary sources are errors in soil moisture retrievals and errors in the land surface model that include model parameterizations (poorly or insufficiently represented processes as well as scale issues) and parameter errors (insufficient calibration). There are also errors in other model forcing fields besides precipitation. Further studies are needed to assess the attribution of these error sources to the total error. Such research will further improve the use of real-time satellite-based precipitation for global flood monitoring.

It is worth noting that the improved precipitation estimates relies heavily on the accuracy of the soil moisture retrievals. The skill in soil moisture retrieved over regions with heavy vegetation is low due to emission from the vegetation and blockage of surface emissions by the vegetation. Improvements in soil moisture retrievals over heavily vegetated regions from lower frequency L-band sensors may help improve the reliability and accuracy of the merged precipitation products. Such an approach may be particularly promising given encouraging soil moisture results from the ESA's Soil Moisture Ocean Salinity (SMOS) mission, and the recently launched NASA Soil Moisture Active Passive (SMAP) mission. On the other hand, the presence of data gaps between overpasses could be a large source of uncertainty in data assimilation. Further effort towards reliable spatial–temporal continuous (gap filled) satellite soil moisture datasets is needed.

While it has been illustrated in this study that the enhancement of real time satellite precipitation estimates can be realized through an assimilation approach using satellite soil moisture data products and a particle filter, additional satellite-based observations (e.g. multi-sensor soil moisture products) or variables (e.g. land surface temperatures as shown in Wanders et al., 2015, inundated area), could be added/replaced in the assimilation process with different levels of complexity; e.g. apply constrains on particle generation. This opens up a great number of opportunities in using space-borne observations for supplementing direct retrievals of precipitation.

HESSD
12, 5749–5787, 2015

Acknowledgements. This research was supported through NASA grant NNX13AG97G (Multi-sensor enhancement of real-time satellite precipitation retrievals for improved drought monitoring) under the Precipitation Measurement Mission. This support is gratefully acknowledged.

References

Brocca, L., Melone, F., Moramarco, T., and Morbidelli, R.: Antecedent wetness conditions based on ERS scatterometer data, J. Hydrol., 364, 73–87, doi:10.1016/j.jhydrol.2008.10.007, 2009.

Brocca, L., Moramarco, T., Melone, F., and Wagner, W.: A new method for rainfall estimation through soil moisture observations, Geophys. Res. Lett., 40, 853–858, doi:10.1002/grl.50173, 2013.

Brocca, L., Ciabatta, L., Massari, C., Moramarco, T., Hahn, S., Hasenauer, S., Kidd, R., Dorigo, W., Wagner, W., and Levizzani, V.: Soil as a natural rain gauge: estimating global rainfall from satellite soil moisture data, J. Geophys. Res.-Atmos., 119, 5128–5141, doi:10.1002/2014JD021489, 2014.

Crow, W. T.: Correcting land surface model predictions for the impact of temporally sparse rainfall rate measurements using an ensemble Kalman filter and surface brightness temperature observations, J. Hydrometeorol., 4, 960–973, 2003.

Crow, W. T., Huffman, G. J., Bindlish, R., and Jackson, T. J.: Improving satellite-based rainfall accumulation estimates using spaceborne surface soil moisture retrievals, J. Hydrometeorol., 10, 199–212, doi:10.1175/2008JHM986.1, 2009.

Crow, W. T., Van Den Berg, M. J., Huffman, G. J., and Pellarin, T.: Correcting rainfall using satellite-based surface soil moisture retrievals: the Soil Moisture Analysis Rainfall Tool (SMART), Water Resour. Res., 47, 1–15, doi:10.1029/2011WR010576, 2011.

Ebert, E. E., Janowiak, J. E., and Kidd, C.: Comparison of near-real-time precipitation estimates from satellite observations and numerical models, B. Am. Meteorol. Soc., 88, 47–64, doi:10.1175/BAMS-88-1-47, 2007.

Ek, M. B., Xia, Y., Wood, E., Sheffield, J., Luo, L., Lettenmaier, D., Livneh, B., Mocko, D., Cosgrove, B., Meng, J., Wei, H., Koren, V., Schaake, J., Mo, K., Fan, Y. and Duan, Q.: North American Land Data Assimilation System Phase 2 (NLDAS-2): Development and Applications, GEWEX Newsl., 21, 5–7, 2011.

HESSD

12, 5749–5787, 2015

Francois, C., Quesney, A., and Ottlé, C.: SAR Data into a coupled land surface–hydrological model using an extended Kalman filter, J. Hydrometeorol., 4, 473–487, doi:10.1175/1525-7541(2003)4<473:SAOESD>2.0.CO;2, 2003.
Gao, H., Tang, Q., Shi, X., Zhu, C., Bohn, T. J., Su, F., Sheffield, J., Pan, M., and Wood, E. F.: Water budget record from Variable Infiltration Capacity (VIC) model, in: Algorithm Theoretical Basis Document for Terrestrial Water Cycle Data Records, in review, 2010.
Huffman, G. J., Bolvin, D. T., Nelkin, E. J., Wolff, D. B., Adler, R. F., Gu, G., Hong, Y., Bowman, K. P., and Stocker, E. F.: The TRMM Multisatellite Precipitation Analysis (TMPA): quasi-global, multiyear, combined-sensor precipitation estimates at fine scales, J. Hydrometeorol., 8, 38–55, doi:10.1175/JHM560.1, 2007.
Huffman, G. J., Adler, R. F., Bolvin, D. T., and Nelkin, E. J.: The TRMM Multi-satellite Precipitation Analysis (TMPA), in: Satellite Rainfall Applications for Surface Hydrology, Springer Netherlands, 3–22, 2010.
Kalman, R. E.: A new approach to linear filtering and prediction problems, J. Basic Eng.-T ASME, 82, 35, doi:10.1115/1.3662552, 1960.
Liang, X., Lettenmaier, D. P., Wood, E. F., and Burges, S. J.: A simple hydrologically based model of land surface water and energy fluxes for general circulation models, J. Geophys. Res., 99, 14415–14428, doi:10.1029/94JD00483, 1994.
Liang, X., Wood, E. F., and Lettenmaier, D. P.: Surface soil moisture parameterization of the VIC-2L model: evaluation and modification, Global Planet. Change, 13, 195–206, doi:10.1016/0921-8181(95)00046-1, 1996.
Massari, C., Brocca, L., Moramarco, T., Tramblay, Y., and Didon Lescot, J.-F.: Potential of soil moisture observations in flood modelling: estimating initial conditions and correcting rainfall, Adv. Water Resour., 74, 44–53, doi:10.1016/j.advwatres.2014.08.004, 2014.
Matgen, P., Fenicia, F., Heitz, S., Plaza, D., de Keyser, R., Pauwels, V. R. N., Wagner, W., and Savenije, H.: Can ASCAT-derived soil wetness indices reduce predictive uncertainty in well-gauged areas? A comparison with in situ observed soil moisture in an assimilation application, Adv. Water Resour., 44, 49–65, doi:10.1016/j.advwatres.2012.03.022, 2012.
McCabe, M. F., Wood, E. F., and Gao, H.: Initial soil moisture retrievals from AMSR-E: multiscale comparison using in situ data and rainfall patterns overs Iowa, Geophys. Res. Lett., 32, 1–4, doi:10.1029/2004GL021222, 2005.

HESSD
12, 5749–5787, 2015

Pan, M. and Wood, E. F.: Data Assimilation for Estimating the Terrestrial Water Budget Using a Constrained Ensemble Kalman Filter, J. Hydrometeorol., 7, 534–547, doi:10.1175/JHM495.1, 2006.

Pan, M., Li, H., and Wood, E. F.: Assessing the skill of satellite-based precipitation estimates in hydrologic applications, Water Resour. Res., 46, W09535, doi:10.1029/2009WR008290, 2010.

Pan, M., Sahoo, A. K., and Wood, E. F.: Improving soil moisture retrievals from a physically-based radiative transfer model, Remote Sens. Environ., 140, 130–140, doi:10.1016/j.rse.2013.08.020, 2014.

Pellarin, T., Ali, A., Chopin, F., Jobard, I., and Bergès, J. C.: Using spaceborne surface soil moisture to constrain satellite precipitation estimates over West Africa, Geophys. Res. Lett., 35, 3–7, doi:10.1029/2007GL032243, 2008.

Pellarin, T., Louvet, S., Gruhier, C., Quantin, G., and Legout, C.: A simple and effective method for correcting soil moisture and precipitation estimates using AMSR-E measurements, Remote Sens. Environ., 136, 28–36, doi:10.1016/j.rse.2013.04.011, 2013.

Robock, A., Luo, L., Wood, E. F., Wen, F., Mitchell, K., Houser, P., Schaake, J., Lohmann, D., Cosgrove, B., Sheffield, J., Duan, Q., Higgins, W., Pinker, R., Tarpley, D., Basara, J., and Crawford, K.: Evaluation of the North American land data assimilation system over the southern Great Plains during the warm season, J. Geophys. Res., 108, 8846, doi:10.1029/2002JD003245, 2003.

Schaake, J. C., Duan, Q. Y., Koren, V., Mitchell, K. E., Houser, P. R., Wood, E. F., Robock, A., Lettenmaier, D. P., Lohmann, D., Cosgrove, B., Sheffield, J., Luo, L. F., Higgins, R. W., Pinker, R. T., and Tarpley, J. D.: An intercomparison of soil moisture fields in the North American land data assimilation system (NLDAS), J. Geophys. Res., 109, D01S90, doi:10.1029/2002jd003309, 2004.

Sorooshian, S.: Commentary-GEWEX (Global Energy and Water Cycle Experiment) at the 2004 Joint Scientific Committee Meeting, GEWEX Newsl., 14, 2, 2004.

Wanders, N., Pan, M., and Wood, E. F.: Correction of real-time satellite precipitation with multi-sensor satellite observations of land surface variables, Remote Sens. Environ., 160, 206–221, doi:10.1016/j.rse.2015.01.016, 2015.

Wu, H., Adler, R. F., Tian, Y., Huffman, G. J., Li, H., and Wang, J.: Real-time global flood estimation using satellite-based precipitation and a coupled land surface and routing model. Water Resour. Res., 50, 2693–2717, doi:10.1002/2013WR014710, 2014.

HESSD
12, 5749–5787, 2015

Table 1. Error statistics of recovered precipitation and effect of surface saturation in the idealized experiment (mm day^{-1}).

[Recovered NLDAS]-[NLDAS]	[3B42RT]-[NLDAS]	0	0 ~ 0.2	0.2 ~ 0.5	0.5 ~ 1.0	1.0 ~ 1.5	1.5 ~ 2	2 ~ 2.5	2.5 ~ 5.0	5.0 ~ 7.5	7.5 ~ 10	10 ~ 15	15 ~ 20	20 ~ 25	> 25
All surface conditions	Bias	0.238	0.196	0.365	0.505	0.706	0.867	1.092	0.672	1.155	1.3	2.508	3.32	3.754	3.949
	MAE	0.402	0.42	0.662	0.858	1.136	1.405	1.704	1.478	2.244	2.63	4.206	5.557	6.698	9.758
Unsaturated surface	Bias	0.231	0.191	0.291	0.403	0.524	0.684	0.822	0.654	1.096	1.268	2.193	2.876	3.137	3.14
	MAE	0.393	0.414	0.587	0.754	0.95	1.213	1.428	1.454	2.167	2.581	3.884	5.108	6.069	8.938
Saturated surface	Bias	2.305	5.055	47.647	42.576	50.667	44.088	59.636	6.832	16.09	9.194	46.466	57.984	65.334	64.093
	MAE	3.345	5.537	48.706	43.728	52.428	46.963	61.851	9.643	21.42	15.007	49.07	60.777	69.534	70.727

HESSD
12, 5749–5787, 2015

Table 2. Error statistics of recovered NLDAS based on ΔSM (with added errors) conditioned on 1st layer soil wetness for the idealized experiment (mm day^{-1}).

[Recovered NLDAS]-[NLDAS] [mm day^{-1}]	[VIC 1st SM] [maximum]* [mm]	< −30	−30 ~ −25	−25 ~ −20	−20 ~ −15	−15 ~ −12	−12 ~ −10	−10 ~ −9	−9 ~ −8	> −8
No error	Median	0.035	0.027	0.023	0.019	0.019	0.026	0.034	0.041	0.159
	IQR	0.140	0.081	0.071	0.071	0.082	0.124	0.206	0.289	1.714
0.5	Median	0.660	0.620	0.539	0.502	0.488	0.474	0.446	0.426	0.095
	IQR	1.045	1.041	1.012	1.060	1.134	1.251	1.432	1.608	2.102
1.0	Median	0.855	1.066	1.079	1.033	0.994	0.965	0.965	0.939	0.659
	IQR	1.523	1.723	1.771	1.829	1.955	2.079	2.143	2.188	2.586
1.5	Median	0.804	1.199	1.370	1.405	1.352	1.269	1.298	1.344	1.168
	IQR	1.726	1.918	1.825	2.289	2.490	2.805	3.265	3.657	3.926
2.0	Median	0.682	1.066	1.404	1.558	1.521	1.438	1.505	1.640	1.539
	IQR	1.756	2.091	2.875	3.447	3.630	3.728	3.729	3.729	3.910
2.5	Median	0.588	0.965	1.366	1.523	1.529	1.505	1.640	1.775	1.775
	IQR	1.588	2.146	3.193	3.646	3.729	3.729	3.736	4.260	5.289
3.0	Median	0.146	0.802	1.198	1.405	1.471	1.505	1.647	1.842	1.878
	IQR	1.357	2.159	3.036	3.729	3.741	3.790	4.335	5.235	5.467
3.5	Median	0.119	0.588	0.965	1.269	1.404	1.471	1.640	1.903	1.959
	IQR	1.449	2.256	2.344	3.799	3.864	3.918	5.181	5.400	5.517
4.0	Median	0.222	0.559	0.830	1.147	1.303	1.404	1.633	1.876	1.972
	IQR	0.992	2.356	2.481	3.985	4.046	4.703	5.527	5.519	5.625
4.5	Median	0.000	0.254	0.673	1.024	1.201	1.336	1.598	1.862	1.926
	IQR	1.700	2.287	2.629	4.200	4.277	5.406	5.713	5.602	6.481
5.0	Median	0.000	0.152	0.516	0.897	1.100	1.269	1.539	1.809	1.886
	IQR	1.623	2.541	2.910	4.428	4.514	5.948	5.903	5.786	7.043

* 1st layer soil depth is 100 mm with a SM capacity of ~ 45 mm depending on porosity.

HESSD
12, 5749–5787, 2015

Table 3. Error statistics of 3B42RT and $3B42RT_{ADJ}$ compared to NLDAS precipitation ($mm\,day^{-1}$).

[3B42RT]-[NLDAS] [$mm\,day^{-1}$]		< −25	−25 ~ −20	−20 ~ −15	−15 ~ −10	−10 ~ −5	−5 ~ −2	−2 ~ −0.5	−0.5 ~ 0.5	0.5 ~ 2	2 ~ 5	5 ~ 10	10 ~ 15	15 ~ 20	20 ~ 25	> 25
[3B42RT]-[NLDAS]	Mean	−32.322	−22.192	−17.126	−12.088	−6.982	−3.221	−1.092	−0.024	1.111	3.196	6.869	11.958	16.965	21.95	27.349
	STD	8.519	1.423	1.422	1.416	1.393	0.848	0.426	0.118	0.426	0.842	1.368	1.387	1.372	1.382	2.078
[$3B42RT_{ADJ}$]-[NLDAS]	Mean	−31.239	−20.307	−14.792	−9.694	−4.805	−1.603	0.16	1.078	0.439	0.209	0.023	−0.061	0.004	−0.033	−0.12
	STD	11.032	6.404	6.116	5.344	4.08	2.732	1.878	1.182	1.857	2.286	2.604	2.907	3.006	2.743	2.407

HESSD
12, 5749–5787, 2015

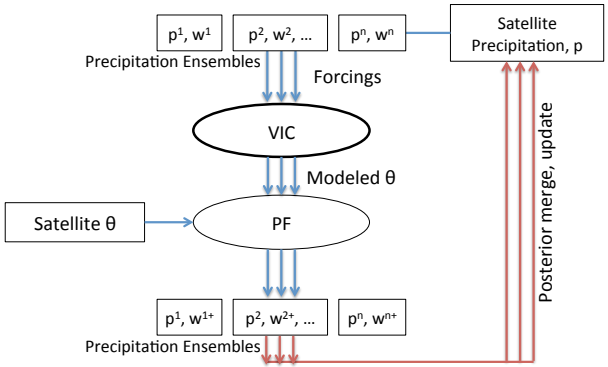

Figure 1. Schematic of particle filtering for dynamic assimilation of AMSR-E/LSMEM ΔSM into TMPA (3B42RT).

HESSD
12, 5749–5787, 2015

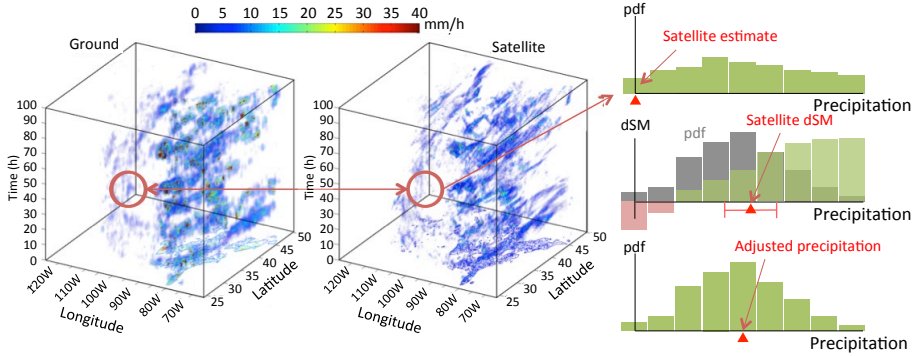

Figure 2. Schematic for handling prior and posterior probability density handling strategy in particle filter.

HESSD
12, 5749–5787, 2015

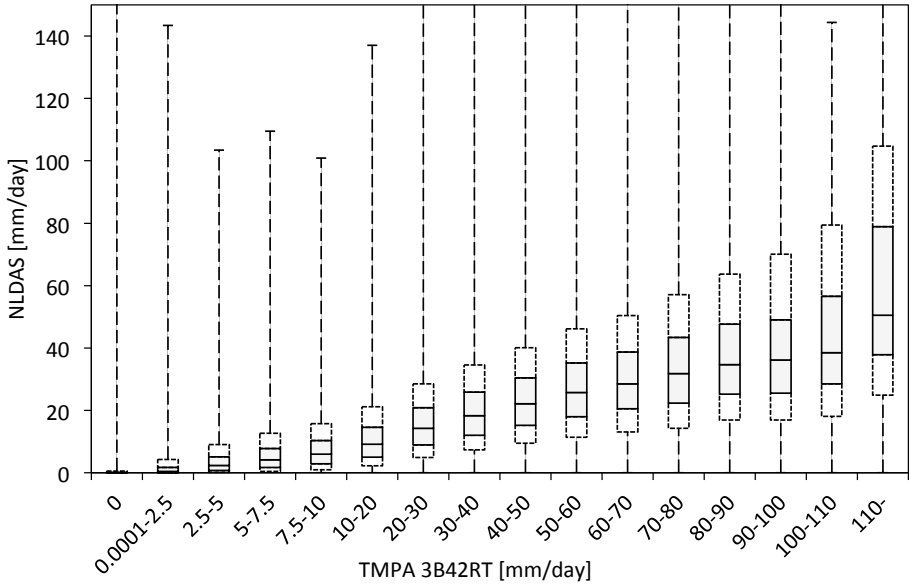

Figure 3. Statistics of NLDAS precipitation given TMPA (3B42RT) precipitation measurement. Boxplot shows the minimum, 15 % quantile, 30 % quantile, median, 70 % quantile, 85 % quantile and maximum value of NLDAS precipitation given TMPA (3B42RT) precipitation in a certain bin.

HESSD
12, 5749–5787, 2015

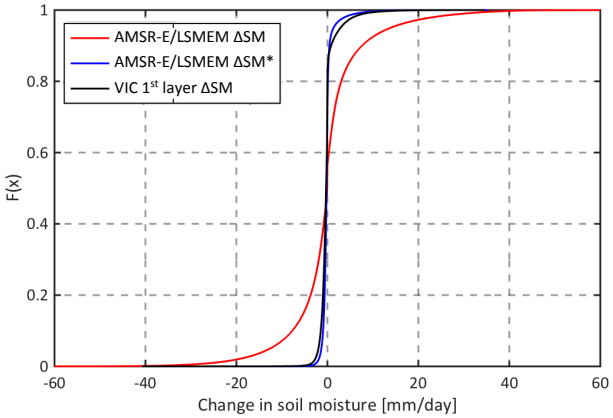

Figure 4. Empirical cumulative distribution function of changes in soil moisture from top layer soil moisture from NLDAS precipitation forced VIC simulation (black), and AMSR-E/LSMEM soil moisture retrieval before (red) and after (blue) pre-processing.

HESSD
12, 5749–5787, 2015

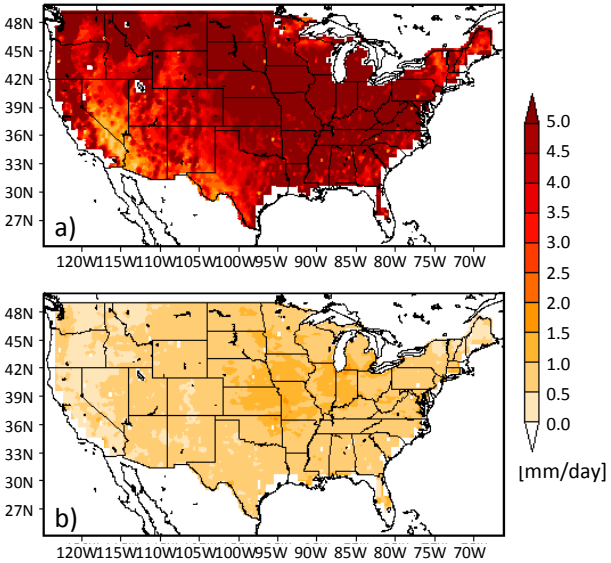

Figure 5. Spatial distribution of mean absolute difference of VIC 1st layer SM and AMSR-E/LSMEM ΔSM, **(a)** before and **(b)** after pre-processing.

HESSD
12, 5749–5787, 2015

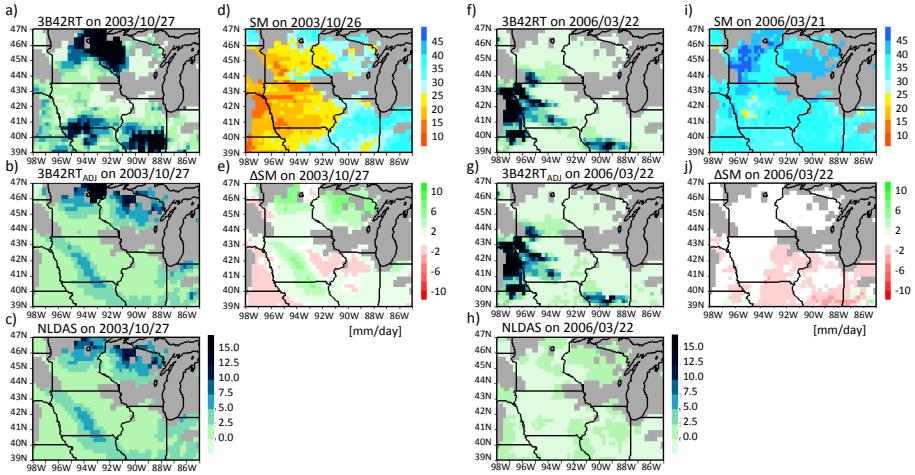

Figure 6. Two cases with recovered spatial rainfall pattern in idealized experiment after merging satellite soil moisture retrieval on: **(a)** 27 October 2003 and **(b)** 22 March 2006.

HESSD
12, 5749–5787, 2015

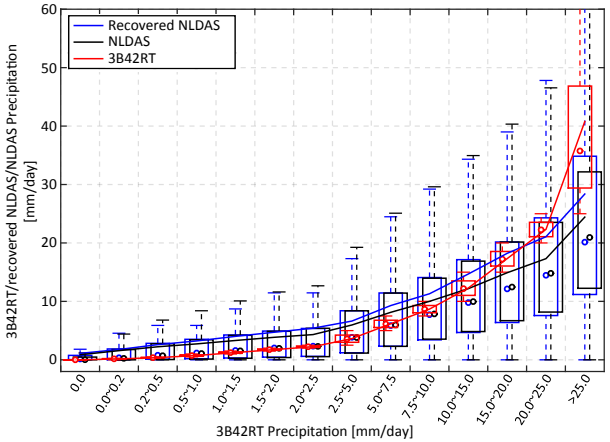

Figure 7. Accuracy of recovered precipitation in idealized experiment.

HESSD
12, 5749–5787, 2015

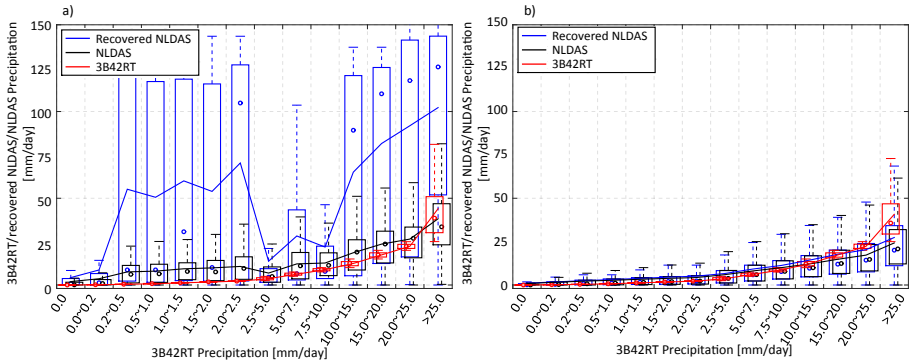

Figure 8. Same as Fig. 7, separately comparing the improvement performance of recovered NLDAS precipitation **(a)** with and **(b)** without surface saturation condition. Statistics provided in Table 1.

HESSD
12, 5749–5787, 2015

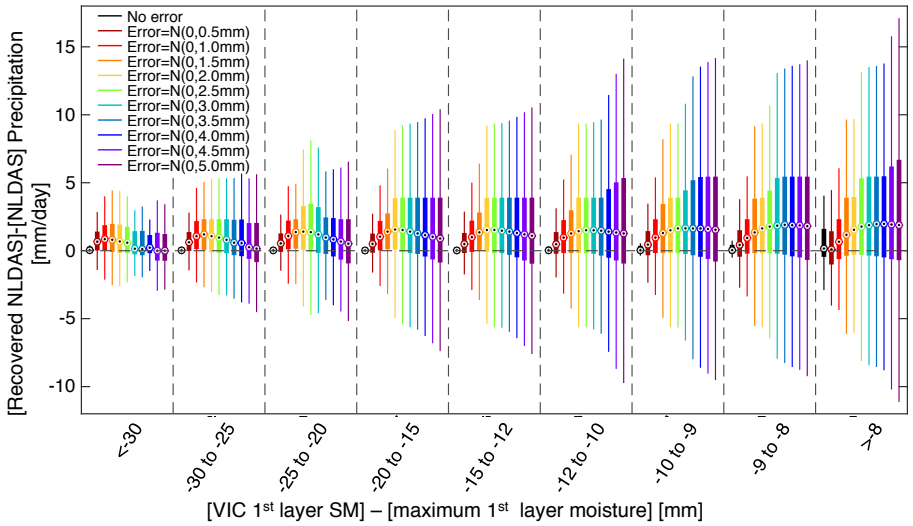

Figure 9. Error in recovered NLDAS precipitation given surface moisture condition. Recovered NLDAS is based on using "truth" soil moisture and soil moisture with normal error: $N(0,0.5\,\text{mm})$, $N(0,1.0\,\text{mm})$, $N(0,1.5\,\text{mm})$, $N(0,2.0\,\text{mm})$, $N(0,2.5\,\text{mm})$, $N(0,3.0\,\text{mm})$, $N(0,3.5\,\text{mm})$, $N(0,4.0\,\text{mm})$, $N(0,4.5\,\text{mm})$ and $N(0,5.0\,\text{mm})$. Statistics provided in Table 2.

HESSD
12, 5749–5787, 2015

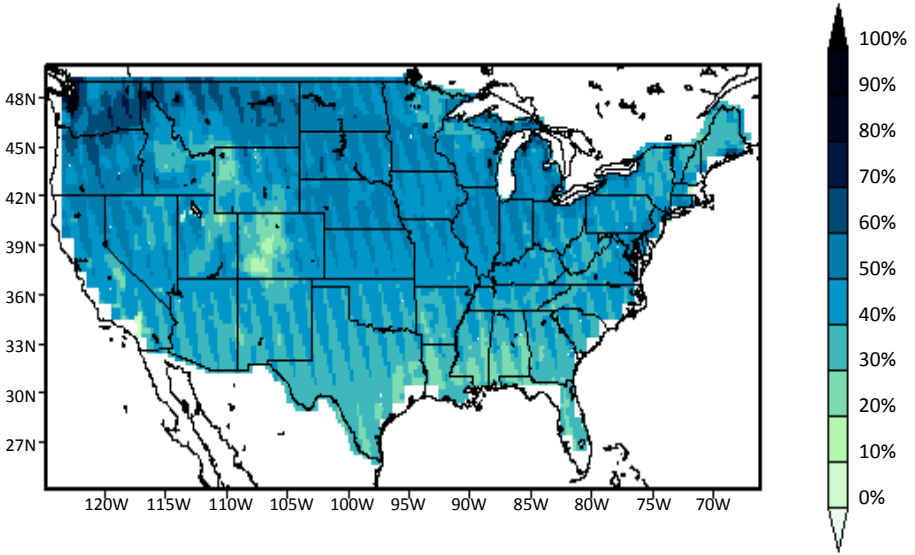

Figure 10. Percentage of time steps with AMSR-E/LSMEM ΔSM observations.

HESSD
12, 5749–5787, 2015

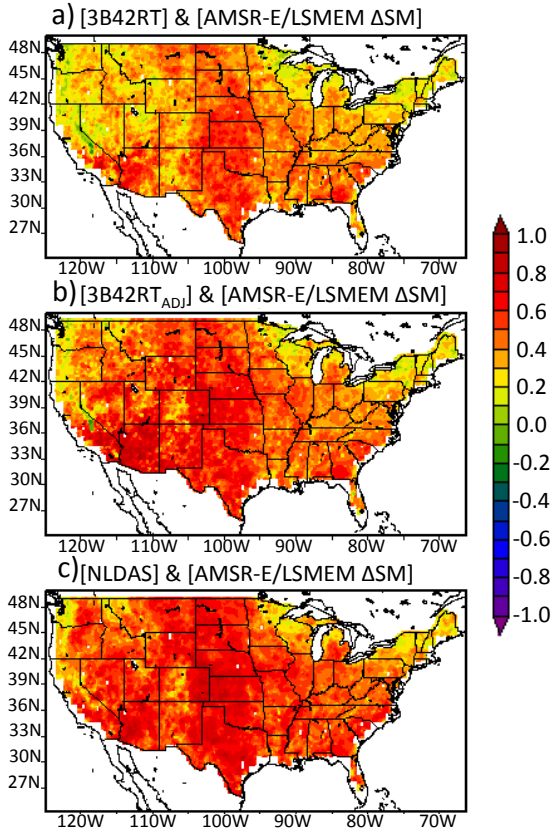

Figure 11. Pearson correlation coefficient between AMSR-E/LSMEM ΔSM and precipitation: **(a)** TMPA (3B42RT), **(b)** TMPA (3B42RT$_{ADJ}$) and **(c)** NLDAS.

HESSD
12, 5749–5787, 2015

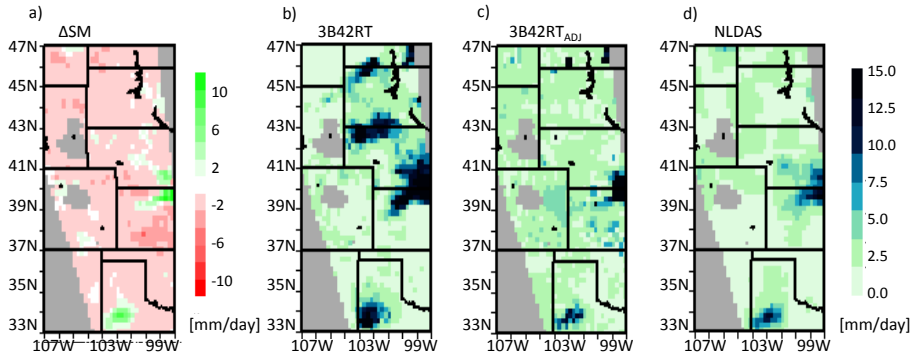

Figure 12. 26 May 2006 Rainfall pattern in TMPA (3B42RT) **(b)** against NLDAS **(d)** as detected by AMSR-E/LSMEM ΔSM **(a)**, and recovered rainfall field TMPA (3B42RT$_{ADJ}$) by assimilating AMSR-E/LSMEM ΔSM into TMPA **(c)**. Gray shading shows area without soil moisture retrievals.

HESSD
12, 5749–5787, 2015

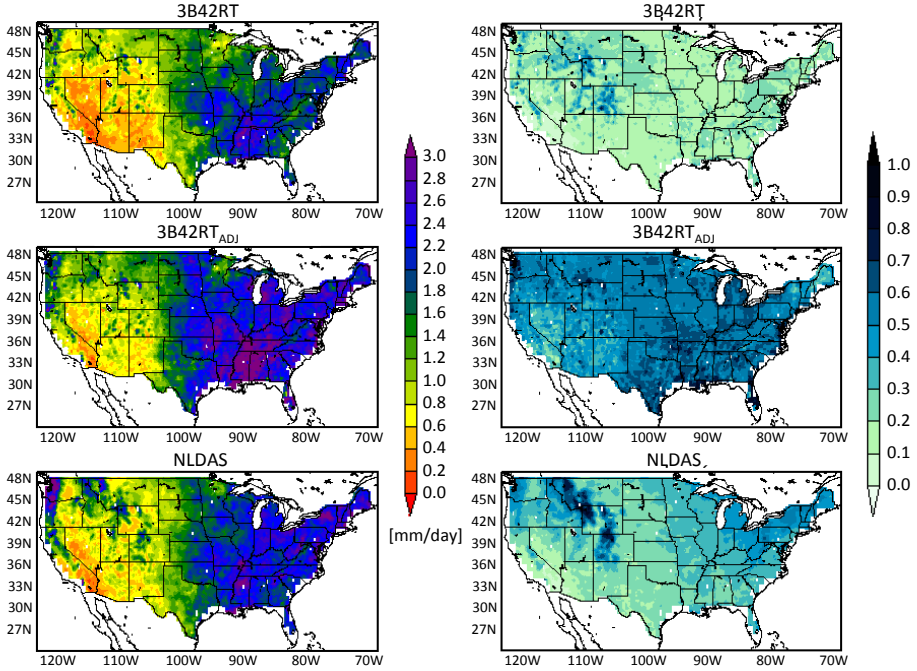

Figure 13. Annual mean precipitation (left) and frequency of days with rain (precipitation > 0.2 mm day^{-1}, right) in TMAP (3B42RT) (top), TMPA (3B42RT$_{ADJ}$) (middle) and NLDAS (bottom) of time steps with AMSR-E/LSMEM ΔSM retrievals.

HESSD
12, 5749–5787, 2015

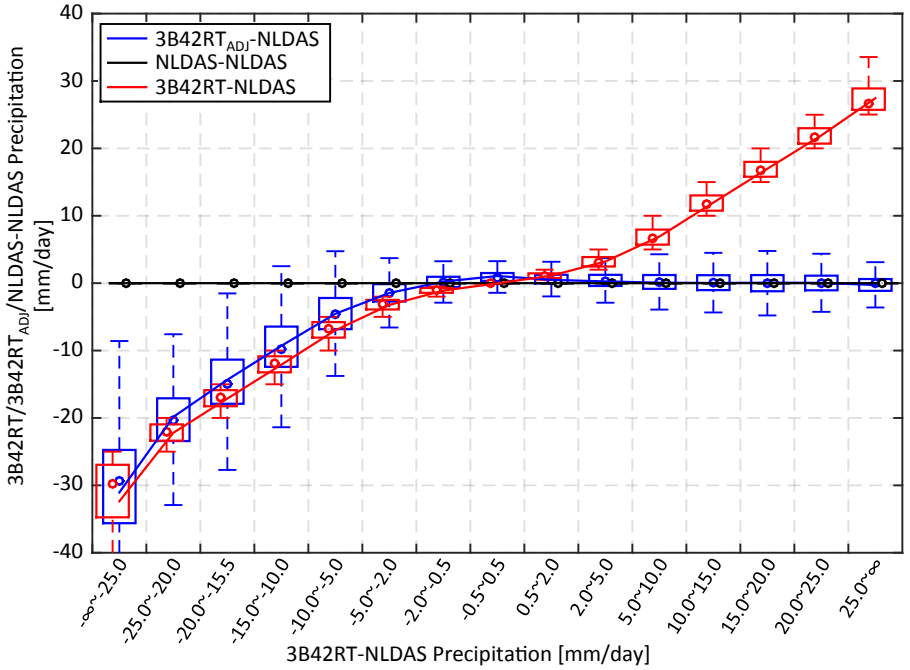

Figure 14. Distribution of updated TMPA (3B42RT) and TMPA (3B42RT$_{ADJ}$) precipitation error compared to NLDAS. Statistics are provided in Table 3.

HESSD
12, 5749–5787, 2015

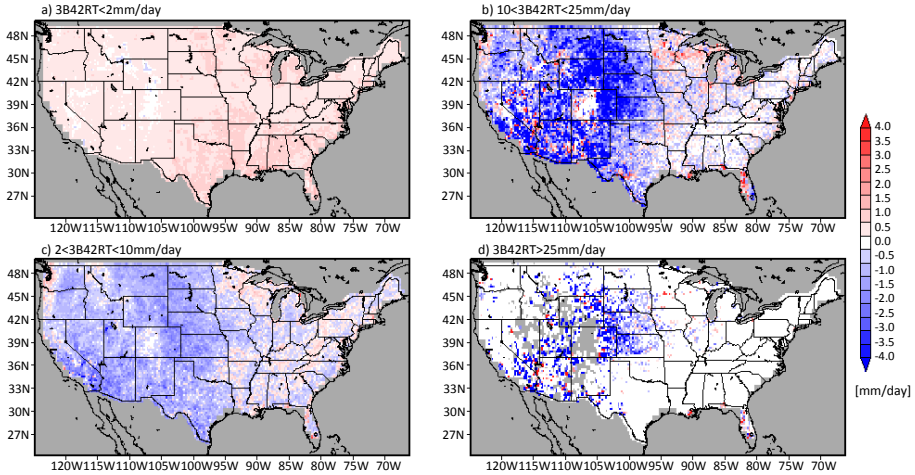

Figure 15. Difference in mean absolute error of TMPA ($3B42RT_{ADJ}$) and TMPA (3B42RT) compared to NLDAS ($MAE(3B42RT_{ADJ})$-MAE(3B42RT)).

HESSD
12, 5749–5787, 2015

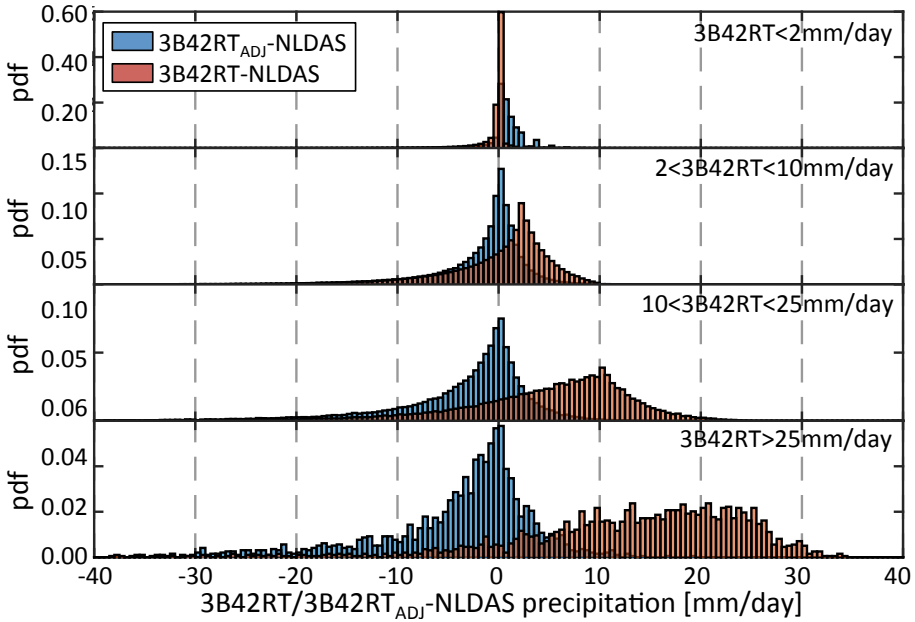

Figure 16. Distribution of TMPA (3B42RT) and TMPA (3B42RT$_{ADJ}$) errors for low vegetated (annual mean LAI < 1.5) and non-mountainous areas (elevation < 1500 m).

HESSD
12, 5749–5787, 2015